Completely Transparent Conducting Oxide-Free and Flexible Dye-Sensitized Solar Cells Fabricated on Plastic Substrates

Kicheon Yoo,[†,‡,#] Jae-Yup Kim,[†,#] Jin Ah Lee,[†] Jin Soo Kim,[§] Doh-Kwon Lee,[†] Kyungkon Kim,[∥] Jin Young Kim,[†,⊥] BongSoo Kim,[†,¶] Honggon Kim,[†] Won Mok Kim,[§] Jong Hak Kim,[‡] and Min Jae Ko*[,†,⊥,▽]

[†]Photo-Electronic Hybrids Research Center and [§]Electronic Materials Research Center, Korea Institute of Science and Technology (KIST), Seoul, 136-791, Republic of Korea, [‡]Department of Chemical and Biomolecular Engineering, Yonsei University, Seoul, 120-746, Republic of Korea, [∥]Department Chemistry and Nano Science and [¶]Department of Science Education, Ewha Womans University, Seoul, 120-750, Republic of Korea, and [⊥]Green School and [▽]KU-KIST Graduate School of Converging Science and Technology, Korea University, Seoul, 136-701, Republic of Korea. [#]K. Yoo and J.-Y. Kim contributed equally to this work.

ABSTRACT To achieve commercialization and widespread application of next-generation photovoltaics, it is important to develop flexible and cost-effective devices. Given this, the elimination of expensive transparent conducting oxides (TCO) and replacement of conventional glass substrates with flexible plastic substrates presents a viable strategy to realize extremely low-cost photovoltaics with a potentially wide applicability. To this end, we report a completely TCO-free and flexible dye-sensitized solar cell (DSSC) fabricated on a plastic substrate using a unique transfer method and back-contact architecture. By adopting unique transfer techniques, the working and counter electrodes were fabricated by transferring high-temperature-annealed TiO_2 and Pt/carbon films, respectively, onto flexible plastic substrates without any exfoliation. The fabricated working electrode with the conventional counter electrode exhibited a record efficiency for flexible DSSCs of 8.10%, despite its TCO-free structure. In addition, the completely TCO-free and flexible DSSC exhibited a remarkable efficiency of 7.27%. Furthermore, by using an organic hole-transporting material (spiro-MeOTAD) with the same transfer method, solid-state flexible TCO-free DSSCs were also successfully fabricated, yielding a promising efficiency of 3.36%.

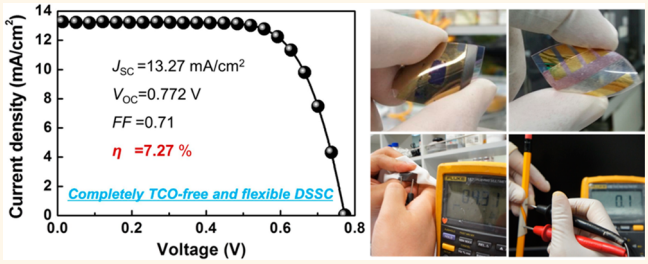

KEYWORDS: dye-sensitized solar cells · TCO-free · flexible · plastic substrates · transfer method

Ever-increasing global energy consumption necessitates the development of advanced renewable energy technologies, among which, solar or photovoltaic (PV) cells offer a number of strategic benefits in terms of their ability to directly convert abundant solar energy into electricity in a clean, quiet, and reliable way. However, the crystalline silicon solar cells that occupy most of the market share today currently supply only a small fraction of the world's energy needs, which is largely because of their high cost compared to conventional energy resources. Consequently, significant research effort has been directed toward the development of next-generation photovoltaics such as thin film solar cells,[1−4] mesoscopic dye-sensitized solar cells (DSSCs),[5−12] and organic solar cells.[13−17] Of these, it is DSSCs that have emerged as the more promising energy source mainly due to their low production cost, ease of fabrication, and possible flexibility.

Conventional DSSCs are fabricated by the high-temperature annealing (over 450 °C) of nanocrystalline TiO_2 electrodes on rigid transparent conducting oxide glass substrates. This particular substrate, however, has a number of drawbacks with regard to its frangibility, weight and rigidity, the latter preventing roll-to-roll mass production and the integration of DSSCs in many portable devices.[18] Replacing this conventional glass substrate with a flexible plastic one compatible with the continuous roll-to-roll process would therefore result in far more

* Address correspondence to mjko@kist.re.kr.

Received for review November 17, 2014 and accepted March 13, 2015.

Published online March 13, 2015
10.1021/acsnano.5b01346

cost-effective, flexible, and lightweight solar cells.[3,4,7,17−23] The handling, installation, and shipping cost in particular would be greatly reduced, and the application of DSSCs could be expanded thanks to the lightweight and nonfragile properties of plastic substrates.[24] However, the preparation of DSSCs on plastic substrates requires low temperatures of ≤150 °C to prevent the thermal degradation of the plastic substrate.[18] This results in poor interconnection between the TiO_2 nanoparticles and an unsuitable pore structure in the working electrode, leading to inferior photovoltaic properties compared to the conventional nonflexible DSSCs based on a high-temperature-annealed electrode.[25] This is currently the biggest problem facing the fabrication of highly efficient flexible DSSCs.

Another important factor in the production cost of DSSCs is the use of transparent conducting oxides (TCOs) such as fluorine-doped tin oxide (FTO) and tin-doped indium oxide (ITO). As these represent about 20−30% of total material costs according to previous reports including "NanoMarkets" (2012),[18,26] the production cost of DSSCs can be substantially reduced if the need for these TCOs can be eliminated. It is also anticipated that the portion of the material price related to TCO/glass substrates will continue to increase as the market for DSSCs and their scale of production become greater. Accordingly, if both the requirement for TCO-free architecture and the use of a plastic substrate can be satisfied simultaneously, an extremely low-cost flexible DSSC with potentially wide-ranging applicability can be realized. However, with the current state of technological development, it is almost impossible to prepare DSSCs that are completely free of TCO and also fabricated on flexible plastic substrates. Those studies that have reported flexible TCO-free DSSCs have mostly used a standard method involving stainless steel meshes and metal foils, resulting in conversion efficiencies of less than 5%.[27−32]

Under these circumstances, we report for the first time a DSSC that is completely TCO-free (*i.e.*, both the working and counter electrodes) and fabricated on a flexible plastic substrate that exhibits a remarkable efficiency and long-term stability by introducing an entirely new architecture and electrode transfer process. This novel transfer process allows high-temperature-annealed TiO_2 electrodes to be embedded in any kind of flexible substrate (*e.g.*, fabric or polymer), with a titanium nitride (TiN) back contact layer filling the role that would otherwise be filled by high-cost TCO.[33] The same transfer process is also used to obtain a TCO-free flexible counter electrode fabricated from a high-temperature-annealed Pt/carbon mixed layer deposited on a plastic substrate. Furthermore, by using an organic hole-transporting material (spiro-MeOTAD) and silver (Ag) nanowire back contact layer with the same transfer method, solid-state TCO-free flexible DSSCs were also successfully fabricated. The photovoltaic performance achieved by using these high-temperature-annealed electrodes was elaborately investigated and is herein discussed in comparison to conventional electrodes.

RESULTS AND DISCUSSION

Figure 1a shows a schematic of the proposed flexible, TCO-free DSSC, the structure of which consists of a mesoporous TiO_2 film (thickness ~10 μm) annealed at high temperature tightly attached to a flexible plastic substrate (polyethylene naphthalate, PEN) using thermal adhesive film (Bynel). A TiN back contact layer deposited on the TiO_2 film serves to collect the generated photoelectrons.[33] This working electrode is assembled with a Pt/carbon mixed layer (thickness ~12 μm) counter electrode, which is attached to the PEN substrate using a Bynel film. The photographs on the right side of Figure 1a show the fabricated working and counter electrode (5 cm × 5 cm) under a bending condition, with both electrodes clearly free of exfoliation and highly flexible. For comparison, schematics of a conventional DSSC and conventional flexible DSSC are provided in Figure 1b. Compared to the conventional flexible DSSC, the most significant difference is that the newly proposed DSSC utilizes a high-temperature-annealed TiO_2 electrode, which is far more favorable for efficient electron transport.[25]

The typical processing steps adopted for the preparation of TCO-free flexible working and counter electrodes are shown in Supporting Information Figure S1a and b, respectively. The working electrode was prepared by depositing a paste containing nanocrystalline TiO_2 particles 20 nm in diameter onto a glass substrate using the doctor blade technique and then annealing this film at 500 °C. These steps are similar to those used in the preparation of conventional nonflexible working electrodes; however, the critical step is successfully transferring this working electrode onto a flexible plastic substrate. For this, the deposited TiO_2 film was first attached to a PEN substrate using a Bynel film, and then the stacked substrates were dipped in 5 wt % aqueous solution of HF for 30 s to detach the glass substrate. During this step, the glass at the TiO_2 film interface slightly dissolved, facilitating its detachment and resulting in the formation of TiO_2/Bynel/PEN. It was confirmed that it is possible to transfer the TiO_2 film without any exfoliation even if a large film size of 10 cm × 10 cm is used (Supporting Information Movie S1). Moreover, although HF treatment was used to ensure the exact detachment of TiO_2 films with complicated shapes (Figure 7), the transfer of a TiO_2 film with a simple rectangular shape can be performed without this HF treatment step (Supporting Information Movie S2). The TiN back contact layer was subsequently deposited onto the TiO_2/Bynel/PEN substrate by radio frequency (RF) magnetron sputtering, with the

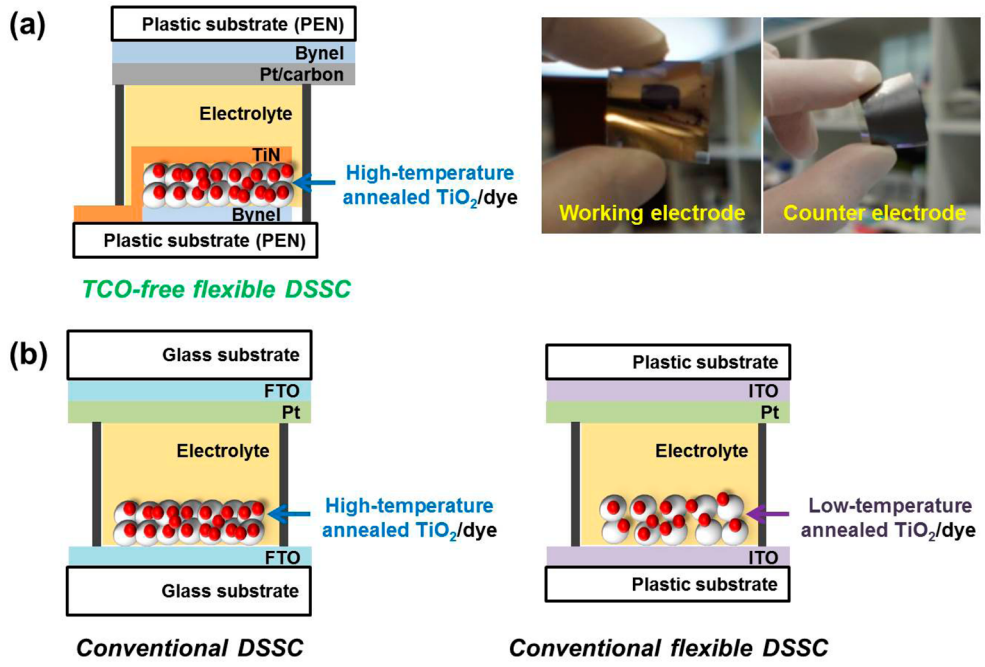

Figure 1. (a) Schematic of a TCO-free flexible DSSC device structure consisting of a flexible PEN substrate, TiN-coated TiO_2 film working electrode, and Pt/carbon layer counter electrode. Photographs on the right side are of the fabricated working and counter electrode (5 cm × 5 cm) under a bending condition. (b) Schematics of conventional DSSC and conventional flexible DSSC device structures.

as-prepared electrode then immersed in ethanol N 719 dye solution for sensitization. It is worth mentioning here that the key feature of the transfer method proposed in this study is its ability to facilitate the fabrication of TiO_2 films annealed at a high temperature, whereas with conventional methods for the preparation of flexible DSSCs such high-temperature annealing needs to be avoided to protect the plastic substrate. This high-temperature annealing is important, as it enhances the interlinking of TiO_2 nanoparticles and thereby improves electron transport in the photoelectrode.[25] Meanwhile, the TiN back contact layer deposited on the TiO_2 film acts as a charge collector and presents an economically viable alternative to the use of TCO.[33]

Following the preparation of the working electrode, the counter electrode was prepared using a similar procedure (Supporting Information Figure S1b). In the first step, a Pt/carbon paste was prepared by blending carbon paste with a Pt precursor solution and deposited onto a glass substrate by the doctor blade technique. After annealing at 500 °C, the prepared Pt/carbon layer was transferred to a flexible PEN substrate by a similar transfer method to that used for the working electrode. The annealing of the Pt/carbon layer improves its electric conductivity, thereby eliminating the need for any additional conductive layers. In addition, both carbon and Pt act as catalysts for the reduction of the iodide-based electrolyte used in DSSC.

Supporting Information Figure S2 compares the overall fabrication process of conventional and TCO-free flexible DSSCs. Compared to the fabrication process of conventional DSSCs, just one additional step is needed for the fabrication of TCO-free flexible DSSCs, meaning that this new approach is sufficiently simple. In addition, we confirmed that mesoporous films can be transferred without any exfoliation or breakage through top and cross-sectional field-emission scanning electron microscope (FE-SEM) images (Section II in the Supporting Information). This is attributed to the relatively weak force of adhesion between the mesoporous films and glass substrate when compared to the interlinking between TiO_2 nanoparticles (or between Pt/carbon particles) afforded by high-temperature annealing. The adhesion between the mesoporous films and PEN substrate is also sufficiently tight, as shown in Figure 2a.

In order to assess the feasibility of the transfer process for use in roll-to-roll mass production, metal foil substrates (stainless steel) were tested in place of glass substrates for the preparation of high-temperature-annealed films (Section II in the Supporting Information). As shown in Supporting Information Figures S7−S10, this found that high-temperature-annealed mesoporous TiO_2 and Pt/carbon films can be successfully transferred from stainless steel to PEN substrates without any discernible degradation of film quality, indicating that this transfer process does indeed have the potential to be used in roll-to-roll mass production.

Figure 2a shows the morphology and structure of the working electrode, as analyzed using FE-SEM; the adhesion at the interface between each component

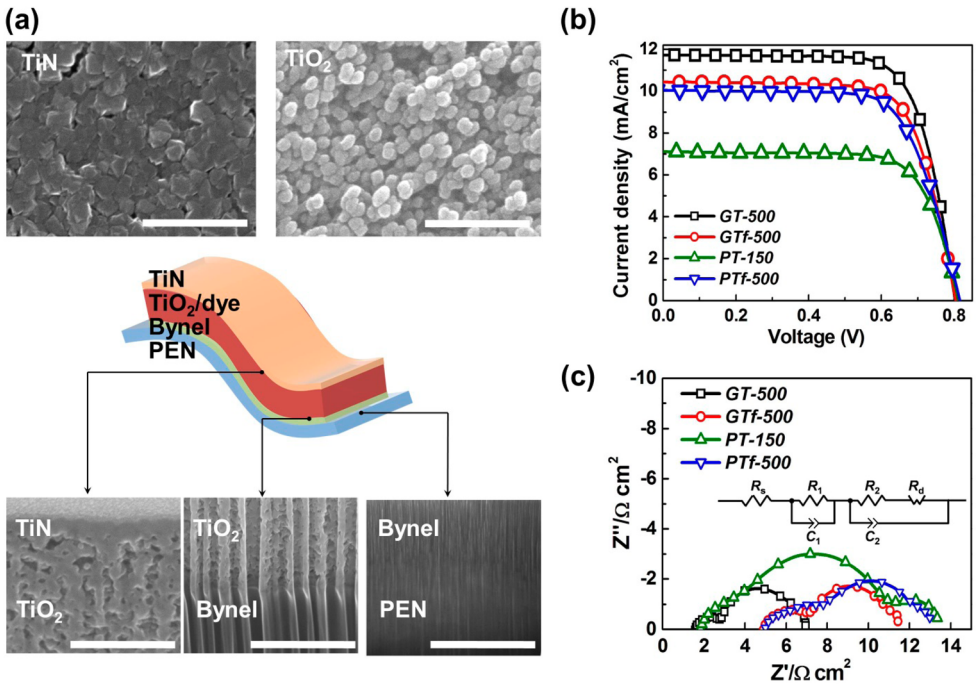

Figure 2. Morphology, structure, and photovoltaic properties of a TCO-free flexible working electrode. (a) FE-SEM images showing the surface (upper images) and cross-sectional (lower images) morphology of the working electrode (all scale bars = 300 nm). (b) *J*−*V* curves of DSSCs fabricated with a conventional nonflexible electrode (GT-500), conventional TCO-free electrode (GTf-500), conventional flexible electrode (PT-150), and TCO-free flexible electrode (PTf-500) under an illuminated state (light intensity: 100 mW/cm^2, AM 1.5G filter). Each electrode was assembled with a conventional Pt/FTO glass counter electrode prepared by thermal decomposition. (c) Impedance spectra of the fabricated DSSCs at an open-circuit potential under AM 1.5G one sun light illumination. The inset shows the equivalent circuit model.

of the working electrode was confirmed by cross-sectional images obtained using a focused ion beam (FIB) system. It can be seen from the SEM images that the TiN layer had a thickness of ~80 nm and was uniformly coated onto the TiO_2 film. Meanwhile, the cross-sectional image confirms that the four layers (*i.e.*, TiN, TiO_2, Bynel, and PEN) all exhibit strong adhesion at the interface (the vertical stripes were formed by the cutting effect of the FIB). The top view of the TiN layer indicates it has a porous surface morphology suitable for the diffusion of electrolyte, whereas the top view of the TiO_2 film obtained before deposition of the TiN layer revealed TiO_2 nanoparticles that were well-interconnected as a result of the high-temperature-annealing conditions.

Figure 2b represents the typical photocurrent density−voltage (*J*−*V*) characteristics of DSSCs employing four different types of working electrodes, namely, a conventional nonflexible electrode (glass/FTO/500 °C-annealed TiO_2 film), conventional TCO-free electrode (glass/500 °C-annealed TiO_2 film/TiN), conventional flexible electrode (PEN/ITO/150 °C-annealed TiO_2 film), and TCO-free flexible electrode (PEN/500 °C-annealed TiO_2 film/TiN), which are hereafter referred to as GT-500, GTf-500, PT-150, and PTf-500, respectively. Each electrode was assembled with a conventional Pt/FTO glass counter electrode prepared by the thermal decomposition method, and their corresponding performance parameters are listed in Supporting Information Table S1. The η of GTf-500 was found to be 6.09%, which is 11.0% less than that of the conventional electrode GT-500 (η = 6.84%). Meanwhile, the η of PT-150 (4.20%) was significantly less (by 38.6%) than that of GT-500. This can be primarily attributed to the poor interconnection between TiO_2 nanoparticles created by low-temperature annealing, as this is unfavorable for electron transport.[25] The PTf-500 prepared by the newly developed transfer method, on the other hand, exhibited an η value of 5.76%, which is 15.8% less than that of a conventional nonflexible electrode (GT-500) and only 5.4% less than that of a conventional TCO-free electrode (GTf-500), despite the use of a plastic substrate. Furthermore, it is 37.1% higher than a conventional flexible electrode (PT-150), despite having a TCO-free structure. This demonstrates that the major limitation of flexible electrodes, namely, the poor interconnection among TiO_2 nanoparticles, can be remarkably improved by this new transfer method.

As shown in Supporting Information Figure S11, the trend observed in the incident photon-to-current efficiency (IPCE) spectra of the samples was in good agreement with the J_{sc} values obtained from their *J*−*V* characteristics. The IPCE of PTf-500 was found to be slightly lower than that of GT-500 and GTf-500, yet much higher than that of PT-150. The reduction of IPCE in the shorter wavelength region (<400 nm) in the case of PT-150 and PTf-500 is attributed to the lower transmittance of PEN than glass in this region (Supporting Information Figure S12).

As an additional check, the photovoltaic performance of PTf-500 was compared to that of a conventional flexible electrode based on a stainless steel substrate (Section IV in the Supporting Information). These stainless steel-based flexible DSSCs were fabricated by depositing a TiO_2 film onto a 100 μm thick stainless steel substrate, annealing at 500 °C, and then assembling this with a conventional Pt/FTO glass counter electrode. The photovoltaic performances of these cells were obtained under back-side illumination and, as shown in Supporting Information Figure S13a and Table S3, revealed the conversion efficiency of stainless steel-based DSSC (η = 5.14%) to be 11% lower compared to PTf-500 (η = 5.76%). This shows the fundamental limitation of back-side illumination, in that light in the low-wavelength region is absorbed by the Pt/FTO counter electrode and electrolyte,[34,35] as confirmed by the IPCE spectra in Supporting Information Figure S13b.

The internal resistance and electron density of each working electrode were also compared by analyzing their electrochemical impedance spectra. Figure 2c shows the Nyquist plots of the DSSCs fabricated using various electrodes, each exhibiting three semicircles in the frequency ranges of 10^6-10^3, 10^3-1, and $1-10^{-2}$ Hz, corresponding to impedance at the counter electrode/electrolyte (R_1), working electrode/electrolyte (R_2), and diffusion resistance of the electrolyte (R_d), respectively.[36,37] The displacement from the origin on the Z' axis represents the series resistance (R_s), which includes both the sheet resistance of the charge collector (TCO or TiN) and contact resistance of the cell.[36] Thus, the value of R_1 could be influenced by the impedance at the charge collector (TCO or TiN)/electrolyte and TiO_2 film/charge collector.[37] The mean electron lifetime (τ_n) in the TiO_2 film was estimated from the reciprocal of the characteristic frequency ($1/\omega_{max}$), the value of ω_{max} being calculated from the relation $\omega_{max} = 2\pi f_{max}$, where f_{max} is the maximum frequency associated with R_2. The spectra were fitted with the equivalent circuit using ZView software, and in addition, the steady-state electron density in the conduction band of TiO_2 was obtained using the following relation:[36−38]

$$R_k = \left(\frac{k_B T}{q^2 A n_s}\right)\left(\frac{1}{Lk}\right) \quad (1)$$

where R_k and k represent the recombination resistance between TiO_2 and electrolyte (R_2) and the reaction rate constant for recombination between TiO_2 and electrolyte, respectively. The variables k_B, T, q, A, n_s, and L represent the Boltzmann constant, absolute temperature, elementary charge, active area of the working electrode, steady-state electron density in the conduction band, and TiO_2 film thickness, respectively. All of the parameters determined using eq 1 are summarized in Supporting Information Table S2. The TCO-free electrodes (GTf-500 and PTf-500) have a higher R_s than GT-500, due to the lower electrical conductivity of the TiN back-contact layer compared to that of the conventional FTO layer. In addition, as a result of the weak interconnection between the TiO_2 film and charge collector, these electrodes showed a higher R_1 value than the GT-500 or PT-150 electrodes.

Notably, the τ_n and n_s values were significantly lower in the case of PT-150 than the other three electrodes. This is due to the low-temperature-annealing conditions adopted during the preparation of PT-150, which could have resulted in many surface states in the TiO_2 film capable of acting as recombination centers.[39] This explains why the τ_n was much less than that of the TiO_2 film prepared by high-temperature annealing (GT-500) and accords well with previous results.[25,39] The measured n_s value of PT-150 was found to be an order of magnitude lower than that of GT-500, and yet, the τ_n and n_s values of PTf-500 were comparable to those of GT-500. This indicates that the poor electrical properties associated with low-temperature annealing are nearly absent in the case of PTf-500. Furthermore, the results derived from the impedance study clearly indicate that PTf-500 exhibits a photovoltaic performance comparable to that of GT-500 and has a much greater performance than PT-150 despite having a TCO-free structure.

Long-term stability tests were performed under light soaking conditions to confirm whether the use of a plastic substrate causes a tendency for the performance to degrade over time. The long-term stability of PTf-500 was compared with that of GTf-500 (Supporting Information Figure S14), through which it was found that GTf-500 and PTf-500 maintain 78% and 70% of their initial conversion efficiency, respectively, after light soaking for 1000 h. Both devices can therefore be considered to exhibit reasonable long-term stability, especially considering the prolonged light soaking condition. This suggests that the use of a plastic substrate does not in fact affect long-term stability, although further studies are needed to achieve even greater stability. In addition, measurement of hardness after the bending test (Section VI in the Supporting Information) found PTf-500 to exhibit excellent flexibility and to be greatly superior to the conventional flexible electrode (PT-150) in this regard. Significantly, the electrical properties of the deposited TiN back-contact layer were maintained even after 1000 bending cycles to a radius of 7 mm (Supporting Information Figure S16).

In order to enhance the conversion efficiency of PTf-500, a light-scattering effect was added by introducing scattering layers that were prepared by mixing TiO_2 particles of 20 and 500 nm in diameter.[40,41] Figure 3a presents a schematic of the proposed high-efficiency TCO-free flexible working electrode, which is labeled as PTf-500S. In this, three separate TiO_2 layers

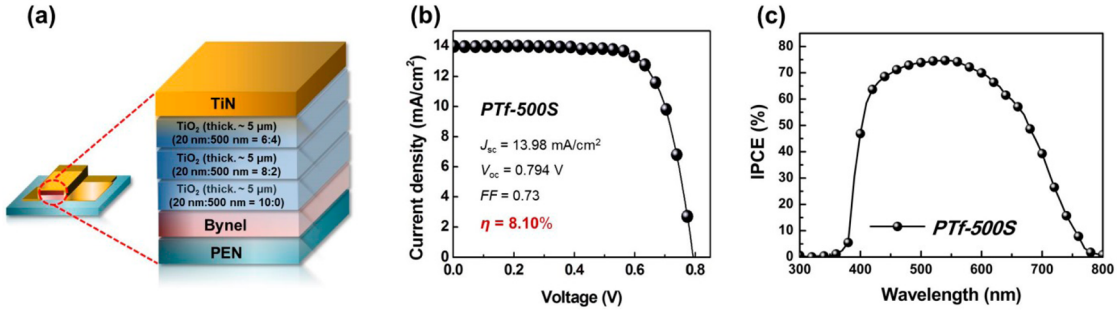

Figure 3. Structure and photovoltaic properties of a high-efficiency, TCO-free, and flexible working electrode. (a) Schematic of the proposed electrode (PTf-500S) showing the three different TiO_2 layers prepared by mixing TiO_2 particles of 20 and 500 nm diameter to ratios of 10:0, 8:2, and 6:4 (w/w). (b) $J-V$ curve obtained under an illuminated state (light intensity: 100 mW/cm^2, AM 1.5G filter, active area: 0.425 cm^2, TiO_2 film thickness: 14.25 μm). (c) IPCE spectrum of a DSSC fabricated using PTf-500S and a conventional Pt/FTO glass counter electrode.

with different ratios of scattering particles are stacked in sequence to maximize the light-scattering effect. Figure 3b shows the $J-V$ characteristics of PTf-500S assembled with a conventional Pt/FTO glass counter electrode, demonstrating a greatly enhanced η value of 8.10% when compared to PTf-500. The J_{sc} value of 13.98 mA/cm^2 was also well matched with the integrated J_{sc} from the IPCE spectrum (13.62 mA/cm^2), as shown in Figure 3c. This is a remarkable result, as to the best of our knowledge, this is the highest conversion efficiency that has ever been achieved for flexible DSSCs, despite its TCO-free structure. The best conversion efficiency that has been achieved to date for flexible DSSCs was 8.07% under one sun condition, with this being obtained from a DSSC fabricated on commercial ITO/PEN substrates.[42]

In order to achieve high efficiency in a completely TCO-free and flexible DSSC, the catalytic performance of the counter electrode must be considered as important as the performance of the working electrode. Most of all, the TCO-free counter electrode must exhibit sufficient electrical conductivity. In this study, Pt/carbon/PEN electrode, which was prepared by the transfer method, was used as the TCO-free flexible counter electrode. Here, the carbon layer acts as an electrical conducting layer, and so the conductivity and specific resistance of the electrode were measured as a function of the thickness of this layer, as shown in Supporting Information Figure S17 (Section VII in the Supporting Information). This identified 12 μm as the optimum carbon layer thickness, which was used to further optimize the catalytic performance by varying the concentration of the mixed Pt precursor solution. As can be seen in the SEM images in Supporting Information Figure S18, the surface morphology of the Pt/carbon/PEN electrodes consisted of a uniform dispersion of ~2 μm diameter carbon grains that were all well connected with each other: a structure that is highly favorable to good electrical conductivity. The cyclic voltammograms (CVs), impedance spectra, and $J-V$ characteristics of the counter electrodes were also analyzed by varying the concentration of Pt precursor solution (Supporting Information Figure S19, Tables S4, S5). As evident from the impedance spectra, the R_s value did not show any significant change in relation to increasing Pt concentration, but the R_{CT} (charge transfer resistance) was greatly reduced. This indicates that an increase in Pt content does not affect the electric conductivity, but does significantly enhance the catalytic activity. This is clearly apparent in the fact that the counter electrode prepared with 0.5 M Pt precursor solution exhibits the highest catalytic activity for the I_3^-/I^- redox electrolyte, as well as superior $J-V$ characteristics when assembled with a conventional working electrode (GT-500). This was therefore considered to be the optimum concentration of Pt precursor solution for achieving the highest possible performance.

The catalytic performance of the TCO-free flexible counter electrode (0.5 M Pt/carbon/PEN) was subsequently compared with the conventional nonflexible counter electrode (Pt/FTO) and the conventional flexible counter electrode (Pt-Ti/ITO/PEN) that is commercially available, but very expensive. It was first confirmed that the Pt/carbon/PEN exhibited electrical properties (conductivity and specific resistance) comparable with those of the conventional counter electrodes (Supporting Information Table S6). Figure 4a compares the CV of each counter electrode considered for the analysis, from which it is apparent that all of the samples exhibited two pairs of redox waves. The more positive pair corresponds to the redox reaction of I_2/I_3^-, while the more negative pair corresponds to the redox reaction of I_3^-/I^-.[43] Focus was given in this instance to the negative pair, since the catalytic reaction at the counter electrode in a DSSC is related to the reduction of I_3^- to I^-. It is also well known that the electrochemical rate constant of a redox reaction is inversely proportional to the peak-to-peak separation (E_{pp}), *i.e.*, separation between the cathodic and anodic peak.[43,44] In this study, E_{pp} was estimated to be 0.58, 0.70, and 0.67 V for Pt/FTO,

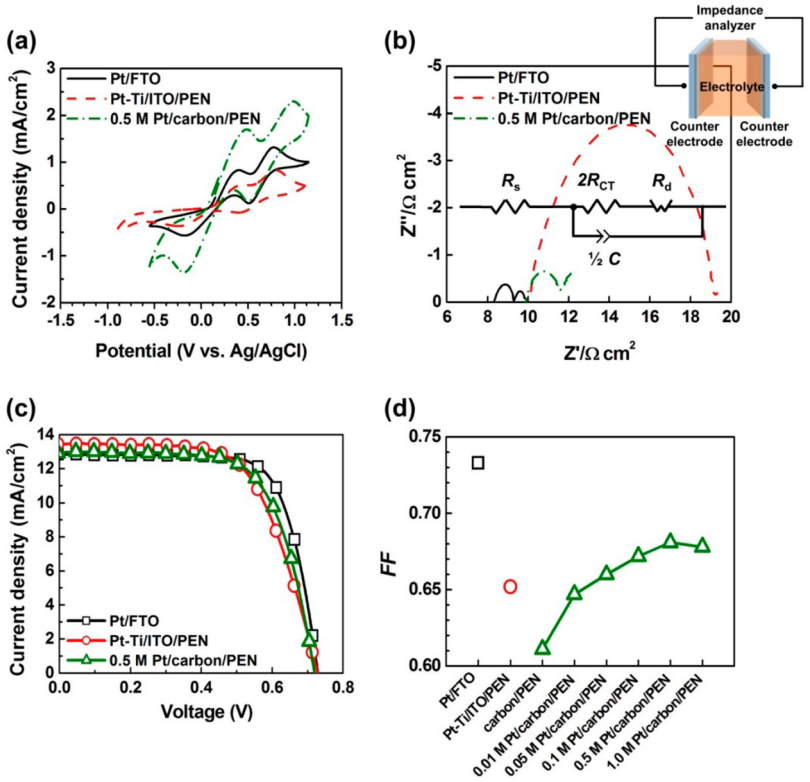

Figure 4. Catalytic performance of a TCO-free flexible counter electrode. (a) Comparison of the cyclic voltammograms (CVs) of a TCO-free flexible counter electrode (0.5 M Pt/carbon/PEN), conventional nonflexible counter electrode (Pt/FTO), and conventional flexible counter electrode (Pt-Ti/ITO/PEN). (b) Impedance spectra of symmetric dummy cells prepared by assembling two identical counter electrodes using hot melt Surlyn. The inset shows the equivalent circuit model, and the figure on the right shows a schematic of the symmetric dummy cell used. (c) *J*−*V* curves of DSSCs using each counter electrode (0.5 M Pt/carbon/PEN, Pt/FTO, and Pt-Ti/ITO/PEN), as measured under an illuminated state (light intensity: 100 mW/cm^2, AM 1.5G filter). The assembled working electrode was a conventional TiO_2 film/FTO glass type (GT-500). (d) Comparison of the fill factor (FF) of DSSCs using each counter electrode.

Pt-Ti/ITO/PEN, and Pt/carbon/PEN, respectively. This indicates that the intrinsic catalytic activity of Pt/carbon/PEN is lower than that of Pt/FTO, but higher than that of Pt-Ti/ITO/PEN; however, Pt/carbon/PEN produces a much higher redox current density for the I_3^-/I^- reaction than the Pt/FTO and Pt-Ti/ITO/PEN electrodes. This can be attributed to the porous and thick structure of the carbon layer creating a much larger accessible surface area.

Impedance studies were also performed using symmetric dummy cells of counter electrodes prepared by assembling two identical counter electrodes, followed by injection of the electrolyte.[45,46] The impedance spectra obtained are presented in Figure 4b, with the impedance parameters listed in Supporting Information Table S7 being determined by fitting these spectra with the equivalent circuit model shown in the inset of Figure 4b. It is clear from these results that the R_s value of the Pt/carbon/PEN electrode is similar to that of the other counter electrodes, indicating that it also has comparable electrical conductivity. The R_{CT} of Pt/carbon/PEN was about 2 times higher than that of Pt/FTO, but was about 6 times lower than that of Pt-Ti/ITO/PEN. This confirms that the catalytic activity of the Pt/carbon/PEN electrode is far superior to that of Pt-Ti/ITO/PEN, despite its TCO-free structure, which is attributed to the higher intrinsic catalytic activity and larger accessible surface area of the Pt/carbon/PEN electrode identified by the CV data. The higher R_d of the Pt/carbon/PEN electrode may be due to the porous and thick structure of its carbon layer. The variation in R_{CT} for each counter electrode is reflected in their respective *J*−*V* characteristics when assembled with a conventional working electrode (*i.e.*, with GT-500). As shown in Figure 4c and Supporting Information Table S8, the η of Pt/carbon/PEN was 7.6% less than that of Pt/FTO, but was 2.3% higher than that of Pt-Ti/ITO/PEN. The critical factor determining η was the fill factor (FF), which noticeably varied depending on the nature of the counter electrode. As shown in Figure 4d, the FF of the DSSC fabricated using a Pt/carbon/PEN electrode varied with the concentration of the Pt precursor solution. Thus, under optimal conditions, the FF of Pt/carbon/PEN was between that of Pt/FTO and Pt-Ti/ITO/PEN and was concordant with the trend of R_{CT}. Since Pt is an expensive material, its loading is an important factor in determining cost effectiveness. The Pt loading was therefore estimated for the

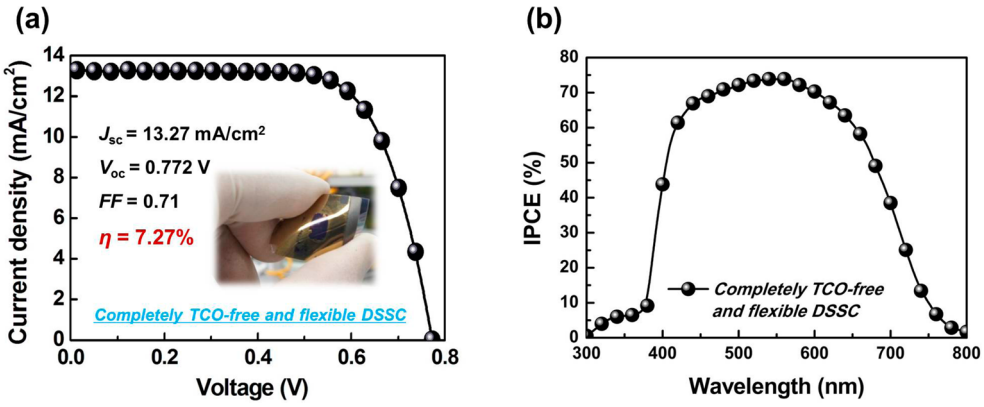

Figure 5. Photovoltaic properties of a completely TCO-free and flexible DSSC. (a) $J-V$ curve obtained under an illuminated state (light intensity: 100 mW/cm^2, AM 1.5G filter, active area: 0.440 cm^2, TiO_2 film thickness: 14.14 μm). (b) IPCE spectrum.

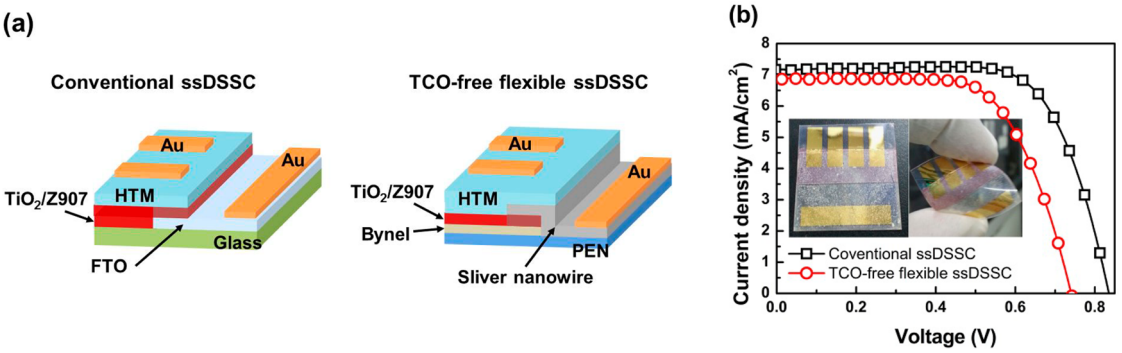

Figure 6. Comparison of (a) the structure and (b) $J-V$ curves obtained under an illuminated state (light intensity: 100 mW/cm^2, AM 1.5G filter) of a conventional ssDSSC and a TCO-free and flexible ssDSSC.

Pt/FTO and Pt/carbon/PEN electrodes from their density and the molar concentration of Pt precursor solution (H_2PtCl_6 solution), as depicted in Section IX in the Supporting Information. On the basis of this estimation, it can be concluded that the flexible TCO-free counter electrode proposed in this study requires only a comparable Pt loading to conventional counter electrodes.

Finally, a completely TCO-free and flexible DSSC was fabricated by assembling the PTf-500S working electrode with the 0.5 M Pt/carbon/PEN counter electrode. Figure 5a shows the $J-V$ characteristics of the resulting DSSC, which achieved a remarkably high η value of 7.27%. Its J_{sc} of 13.27 mA/cm^2 was also well matched with the integrated J_{sc} from the IPCE spectrum (13.22 mA/cm^2) shown in Figure 5b. In order to demonstrate the feasibility of applying this same transfer process and device structure to a solid-state photovoltaic device, spiro-MeOTAD was used as a hole-transporting material in place of a liquid electrolyte to fabricate a flexible, TCO-free solid-state DSSC. The structure of this is shown in Figure 6a in comparison to a conventional ssDSSC and was achieved by transferring a high-temperature-annealed mesoporous TiO_2 film (thickness ~2.5 μm) onto a PEN substrate using Bynel. Since a TiN layer did not provide a sufficiently large pore size for the spiro-MeOTAD to infiltrate into the mesoporous TiO_2 film, Ag nanowires (diameter ~115 nm, length ~20−50 μm) deposited by spin coating were used as the back contact layer instead. As shown in Supporting Information Figure S20, these Ag nanowires were homogeneously deposited onto the mesoporous TiO_2 film to create macropores, through which the spiro-MeOTAD could easily penetrate. Electron probe microanalysis (EPMA, Supporting Information Figure S21) confirmed that carbon was homogeneously dispersed throughout the cross-section of the mesoporous TiO_2 film, implying that the spiro-MeOTAD was sufficient infiltrated. The Ag nanowire back-contact layer also exhibited excellent electrical properties (conductivity: 4.09×10^3 S/cm, specific resistance: 2.45×10^{-4} Ω cm), which were confirmed by 4-point probe measurement. Figure 6b presents the $J-V$ characteristics of the conventional and TCO-free flexible ssDSSCs, while the corresponding performance parameters are listed in Supporting Information Table S10. The η values of the conventional and TCO-free flexible ssDSSC were 4.28% and 3.36%, respectively, meaning that there was little discrepancy in conversion efficiency despite the new structure's absence of TCO and added flexibility. This implies that the transfer method and back-contact architecture proposed in this study are sufficiently compatible with solid-state photovoltaic devices.

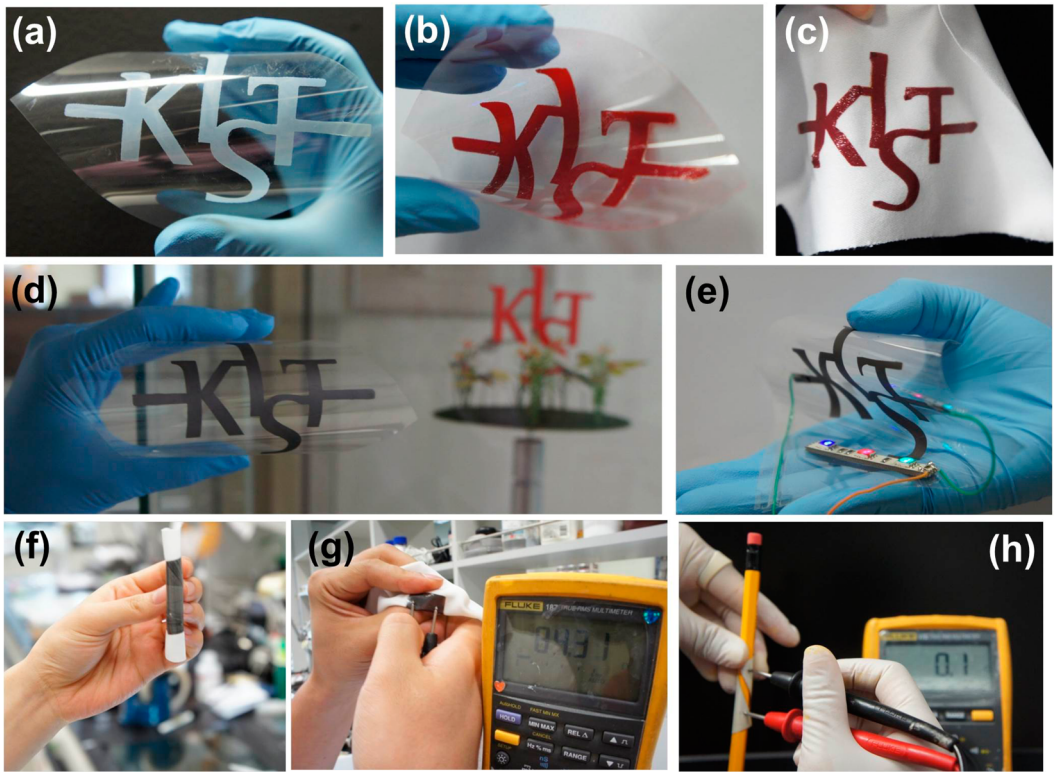

Figure 7. Electrodes prepared on various flexible substrates to a predesigned shape using the transfer method. (a) Nanocrystalline TiO_2 electrode deposited onto OHP film (10 cm × 10 cm). (b) TiO_2 electrode on OHP film after dye adsorption. (c) Dyed TiO_2 electrode deposited on fabric (10 cm × 10 cm, 100% polyester wipe). (d) Pt/carbon electrode prepared on OHP film (10 cm × 10 cm). (e) Pt/carbon electrode on OHP film under a bending condition. The electrical conductivity of the electrode was evaluated by connecting it to a power supply and LED light, its performance being maintained under a bending condition. (f) Pt/carbon electrode prepared on fabric (5 cm × 5 cm, 100% polyester wipe). (g) Electrical conductivity of the Pt/carbon electrode on fabric, as measured using a multimeter. (h) Ag-paste film transferred onto a thermal adhesive film (5 cm × 5 cm, Bynel) after high-temperature annealing (500 °C). The resistance between each end was 0.1 Ω under bending conditions.

To the best of our knowledge, this is the first demonstration of a DSSC that satisfies simultaneously the conditions of being TCO-free and flexible and using a solid-state hole transporting material (HTM) layer. In addition, the Ag nanowires used as a back-contact layer present a promising alternative to TCO materials due to their low cost, superior flexibility, and compatibility with solution-based processes.[47,48] Thus, the results demonstrate that the transfer method and device structure proposed in this study can be readily applied to various devices with various kinds of back-contact materials using vacuum- and solution-based processes. Furthermore, as perovskite solar cells have a similar device structure to ssDSSCs and utilize spiro-MeOTAD as a HTM,[49,50] it should be possible to fabricate flexible, TCO-free perovskite solar cells using this same transfer method and back-contact architecture. Further work is therefore under way to develop flexible, TCO-free solid-state photovoltaics with an even higher conversion efficiency than has been achieved here.

Finally, the reliability of the transfer method adopted in this study was tested by depositing films onto various large-area (10 cm × 10 cm) substrates such as overhead projector (OHP) film and fabric (polyester wipes). Figure 7 shows various electrodes prepared on an OHP film and fabric, which included dyed TiO_2, Pt/carbon, and metal (Ag) electrodes. These deposited films remained exfoliation-free and maintained their electrical conductivity when under a bending condition, indicating that the transfer method proposed in this study can be applied to the fabrication of not only DSSCs but also other types of flexible solar cells or flexible electronic devices.

CONCLUSION

This study has succeeded in developing a completely TCO-free and flexible DSSC with a conversion efficiency of 7.27% by using an original transfer method. As part of this, a high-temperature-annealed TiO_2 electrode and Pt/carbon electrode were successfully transferred onto flexible PEN substrates to form the working and counter electrode, respectively. Systematic analysis of the fabricated DSSC indicated that it has superior photovoltaic properties to DSSCs based on conventional flexible electrodes. In addition, the TCO-free flexible working electrode exhibited a satisfactory long-term stability under light soaking.

This combination of high efficiency, long-term stability, and extremely low fabrication cost represents a significant advancement in DSSC technology, with a great potential for commercialization and widespread application. Furthermore, we believe that the transfer method adopted in this study has the potential to be effectively extended to other types of solar cells or electronic devices that need to be both TCO-free and flexible.

METHODS

Preparation of TiO_2 Paste. To fabricate the working electrodes, a TiO_2 paste was first prepared using nanocrystalline TiO_2 particles of diameter 20 nm, as described in our previous paper.[39] In a typical process, TiO_2 nanoparticles were synthesized by hydrolyzing titanium isopropoxide (97%, Aldrich) in the presence of acetic acid, which was followed by heating at 230 °C for 12 h in a sealed autoclave. Next, ethyl cellulose (Aldrich), lauric acid (Fluka), and terpineol (Fluka) were added, and the ethanol was subsequently removed using a rotary evaporator to obtain a viscous paste. The weight ratio of the final composition was as follows: TiO_2/terpineol/ethyl cellulose/lauric acid = 0.18:0.75:0.05:0.02. Light-scattering pastes were prepared by mixing TiO_2 particles 20 and 500 nm in diameter to a ratio of 8:2 or 6:4 (w/w), with all other constituents being identical to those of the standard TiO_2 paste. The 500 nm TiO_2 particles were purchased from Showa Denko (G2, Japan). For low-temperature annealing, binder-free pastes were also prepared by blending TiO_2 nanoparticles of different diameters (5:20:320 nm = 1:4.5:2.5 wt %); the 5 nm diameter TiO_2 particles were synthesized by a typical sol−gel process, as described in our previous papers.[20−22] The 320 nm diameter nanoparticles were purchased from K. K. Titan (Japan) and then dissolved in ethanol at a concentration of ∼15 wt %.

Preparation of Working Electrodes. The working electrode was fabricated by depositing the preprepared TiO_2 paste onto a glass substrate using the doctor blade technique and then annealing in air at 500 °C for 30 min. The high-efficiency working electrode was prepared by depositing in sequence the three different pastes containing TiO_2 particles of 20 and 500 nm in diameter (20:500 nm = 10:0, 8:2, 6:4, respectively) onto a glass substrate, which was again followed by annealing at the same conditions. The thickness of the TiO_2 film obtained was determined using an Alpha-Step IQ surface profiler (KLA Tencor). Following this, a polyethylene naphthalate substrate (PEN; Teijin Dupont Films, 200 μm thickness) was attached to the TiO_2 film using hot-melt Bynel (Dupont, 25 μm thickness). For this, the hot-melt Bynel and plastic substrate were first stacked onto the TiO_2 film in sequence and then compressed at a pressure of 0.12 MPa at 130 °C for 10 s. The glass substrate was then detached by dipping in a 5 wt % aqueous solution of HF for 30 s, leaving behind the TiO_2 film on a flexible PEN substrate. A TiN back-contact layer was then deposited onto the TiO_2 film by radio frequenc magnetron sputtering of a Ti target under N_2/Ar (2:98 v/v) atmosphere at ambient temperature. Finally, the prepared electrodes were immersed in an ethanol solution containing 0.5 mM *cis*-bis(isothiocyanato)bis(2,2′-bipyridyl-4,4′-dicarboxylato)ruthenium(II)bistetrabutylammonium (N 719, Everlight) at ambient temperature for 24 h. For comparison, a conventional nonflexible working electrode and conventional flexible working electrode were also fabricated. The nonflexible electrode was prepared by depositing the TiO_2 paste onto FTO glass (Pilkington, TEC-8, 8 Ω/square), followed by annealing in air at 500 °C for 30 min. The flexible working electrode was prepared by depositing binder-free TiO_2 paste onto an ITO/polyethylene terephthalate (PEN) substrate (Peccell Technologies Inc., 15 Ω/square, 200 μm thickness), followed by drying in an oven at 150 °C for 30 min. For all electrodes, the dye dipping time was 24 h at ambient temperature.

Preparation of Counter Electrodes. A Pt/carbon paste was prepared by blending carbon paste (Elcocarb C/SP, Solaronix) with H_2PtCl_6 solution in 2-propanol to a ratio of 9:1 (w/w). This was then deposited onto a glass substrate by the doctor blading technique and annealed in air at 500 °C for 30 min. The thickness of the Pt/carbon film obtained in this manner was ∼12 μm. This Pt/carbon layer was subsequently transferred onto a PEN substrate by the same transfer method used for the preparation of the working electrode. For comparison, conventional nonflexible Pt counter electrodes and flexible counter electrodes were also analyzed. The nonflexible Pt electrode was prepared by thermal decomposition, wherein a drop of 7 mM H_2PtCl_6 in 2-propanol was spread over an FTO-coated glass substrate and annealed in air at 400 °C for 10 min. The conventional flexible counter electrode, consisting of Pt−Ti alloy on a PEN substrate (5 Ω/square, 188 μm thickness), was purchased from Peccell Technologies Inc.

Device Fabrication. The working and counter electrodes were sealed and assembled using hot-melt Surlyn of 60 μm in thickness (Dupont 1702). The redox electrolyte consisted of 0.7 M 1-propyl-3-methylimidazolium iodide, 0.03 M I_2, 0.05 M guanidinium thiocyanate, and 0.5 M 4-*tert*-butylpyridine (tBP) in a mixture of acetonitrile and valeronitrile (v/v = 85:15). For all cells, the active area was measured as being within a range of 0.43 ± 0.05 cm^2 using an image analysis program and CCD camera (Moticam 1000). Each cell was covered with a black mask with an aperture to screen any additional illumination through the lateral space.[51]

Preparation of Solid-State Dye-Sensitized Solar Cells (ssDSSCs). Conventional ssDSSCs were fabricated on a laser-patterned FTO-coated glass substrate that had been pretreated by spin coating a 7.5 wt % solution of Ti(IV) bis(ethyl acetoacetato)-diisopropoxide in 1-butanol to form a dense blocking layer, which was then annealed at 125 °C for 5 min. A TiO_2 paste was then deposited using the doctor blade technique and annealed in air at 500 °C for 30 min. The annealed electrodes were then immersed for 16 h in a dye solution of 0.3 mM *cis*-diisothiocyanato(2,2′-bipyridyl-4,4′-dicarboxylic acid)(2,2′-bipyridyl-4,4′-dinonyl)ruthenium(II) (Z 907, Everlight) in a mixture of acetonitrile and *tert*-butanol (v/v = 1:1) at ambient temperature. Onto these dye-coated TiO_2 films, a hole-transporting material solution consisting of 0.13 M 2,2′,7,7′-tetrakis(*N*,*N*-dimethoxyphenylamine)-9,9-spirobifluorene (Spiro-MeOTAD), 21 mM lithium bis(trifluoromethylsulfonyl)imide salt, and 0.11 M tBP in anhydrous chlorobenzene was deposited by spin coating. Finally, gold (Au) back-contacts (150 nm thickness) were deposited by thermal evaporation. In order to fabricate TCO-free flexible ssDSSCs, the TiO_2 paste was first deposited onto a glass substrate and then transferred onto a PEN substrate. Silver (Ag) nanowires suspended in 2-propanol (diameter: 115 nm, length: 20−50 μm, Aldrich) were then deposited as a back-contact layer by spin coating at 1000 rpm for 10 s, a process that was repeated five times. An HTM layer and Au back-contacts were then deposited using the identical process to that used for the conventional ssDSSCs.

Characterization. The morphology of the films was characterized by FE-SEM (Hitachi S4100). Cyclic voltammetry was carried out using a CHI440 potentiostat-galvanostat (CH Instruments Inc.) at a scan rate of 50 mV/s and with an electrolyte consisting of 10 mM LiI, 1 mM I_2, and 0.1 M $LiClO_4$ in acetonitrile. Pt/FTO, Pt/carbon/PEN, and Pt/ITO substrates were used as working electrodes. A saturated calomel electrode and a Pt foil were used as reference electrode and counter electrode, respectively. Photocurrent density−voltage (*J*−*V*) measurements were performed using a Keithley model 2400 Source Measure unit. A 180 W xenon lamp (Yamashita Denso YSS-50A) served as the light source, the intensity of which was adjusted to approximately AM 1.5G one sun light intensity using an NREL-calibrated Si solar cell equipped with a KG-1 filter. The incident photon-to-electron conversion efficiency was measured as a function of wavelength from 350 to 800 nm using a specially designed system for dye-sensitized solar cells (PV Measurements, Inc.).

Electrical impedance spectra were obtained using an impedance analyzer (Solartron 1287) at an open-circuit potential under AM 1.5G one sun light illumination at frequencies ranging from 10^{-2} to 10^{6} Hz. The magnitude of the alternative signal was 10 mV. Impedance parameters were determined by fitting with ZView software. For impedance analysis of each counter electrode, symmetric dummy cells were prepared by assembling two identical counter electrodes using hot-melt Surlyn. The electrical properties were then measured using a 4-point probe electrical measurement system (Mitsubishi Chemical Analytech, MCP-T610).

Conflict of Interest: The authors declare no competing financial interest.

Acknowledgment. The authors acknowledge funding support from the Global Frontier R&D Program on Center for Multiscale Energy System (2012M3A6A7054856) and 2014 University-Institute cooperation program funded by the National Research Foundation under the Ministry of Science, ICT & Future Planning, Korea. This work was also supported by the KIST institutional programs (2 V03780 and 2E25392) and the New & Renewable Energy Program of the Korea Institute of Energy Technology Evaluation and Planning (KETEP) grant (2010T100100651) funded by the Ministry of Trade, Industry & Energy (MOTIE).

Supporting Information Available: Additional data and discussion; movies showing the transfer process. This material is available free of charge *via* the Internet at http://pubs.acs.org.

REFERENCES AND NOTES

1. Jackson, P.; Hariskos, D.; Lotter, E.; Paetel, S.; Wuerz, R.; Menner, R.; Wischmann, W.; Powalla, M. New World Record Efficiency for Cu(In,Ga)Se_2 Thin-Film Solar Cells Beyond 20%. *Prog. Photovoltaics* **2011**, *19*, 894–897.
2. Chiril, A.; Buecheler, S.; Pianezzi, F.; Bloesch, P.; Gretener, C.; Uhl, A. R.; Fella, C.; Kranz, L.; Perrenoud, J.; Seyrling, S.; *et al*. Highly Efficient Cu(In,Ga)Se_2 Solar Cells Grown on Flexible Polymer Films. *Nat. Mater.* **2011**, *10*, 857–861.
3. Fan, Z.; Razavi, H.; Do, J.-W.; Moriwaki, A.; Ergen, O.; Chueh, Y.-L.; Leu, P.; Ho, J. C.; Takahashi, T.; Reichertz, L. A.; *et al*. A Three-Dimensional Nanopillar-Array Photovoltaics on Low-Cost and Flexible Substrates. *Nat. Mater.* **2009**, *8*, 648–653.
4. Lee, C. H.; Kim, D. R.; Cho, I. S.; William, N.; Wang, Q.; Zheng, X. Peel-and-Stick: Fabricating Thin Film Solar Cell on Universal Substrates. *Sci. Rep.* **2012**, *2*, 1000.
5. O'Regan, B.; Grätzel, M. A Low-Cost, High-Efficiency Solar Cell Based on Dye-Sensitized Colloidal TiO_2 Films. *Nature* **1991**, *353*, 737–740.
6. Yella, A.; Lee, H. W.; Tsao, H. N.; Yi, C.; Chandiran, A. K.; Nazeeruddin, M. K.; Diau, E. W.; Yeh, C. Y.; Zakeeruddin, S. M.; Gratzel, M. Porphyrin-Sensitized Solar Cells with Cobalt (II/III)-Based Redox Electrolyte Exceed 12% Efficiency. *Science* **2011**, *334*, 629–634.
7. Durr, M.; Schmid, A.; Obermaier, M.; Rosselli, S.; Yasuda, A.; Nelles, G. Low-Temperature Fabrication of Dye-Sensitized Solar Cells by Transfer of Composite Porous Layers. *Nat. Mater.* **2005**, *4*, 607–611.
8. Ito, S.; Zakeeruddin, S. M.; Comte, P.; Liska, P.; Kuang, D.; Grätzel, M. Bifacial Dye-Sensitized Solar Cells Based on an Ionic Liquid Electrolyte. *Nat. Photonics* **2008**, *2*, 693–698.
9. Lee, K.; Park, S.; Ko, M. J.; Kim, K.; Park, N.-G. Selective Positioning of Organic Dyes in a Mesoporous Inorganic Oxide Film. *Nat. Mater.* **2009**, *8*, 665–671.
10. Hagfeldt, A.; Boschloo, G.; Sun, L.; Kloo, L.; Pettersson, H. Dye-Sensitized Solar Cells. *Chem. Rev.* **2010**, *110*, 6595–6663.
11. Heo, J. H.; Im, S. H.; Noh, J. H.; Mandal, T. N.; Lim, C.-S.; Chang, J. A.; Lee, Y. H.; Kim, H.; Sarkar, A.; Nazeeruddin, M. K.; *et al*. Efficient Inorganic-Organic Hybrid Heterojunction Solar Cells Containing Perovskite Compound and Polymeric Hole Conductors. *Nat. Photonics* **2013**, *7*, 486–491.
12. Burschka, J.; Pellet, N.; Moon, S. J.; Humphry-Baker, R.; Gao, P.; Nazeeruddin, M. K.; Gratzel, M. Sequential Deposition as a Route to High-Performance Perovskite-Sensitized Solar Cells. *Nature* **2013**, *499*, 316–319.
13. Oosterhout, S. D.; M.Wienk, M.; Bavel, S. S. v.; Thiedmann, R.; Koster, L. J. A.; Gilot, J.; Loos, J.; Schmidt, V.; Janssen, R. A. J. The Effect of Three-Dimensional Morphology on the Efficiency of Hybrid Polymer Solar Cells. *Nat. Mater.* **2009**, *8*, 818–824.
14. Yuan, Y.; Reece, T. J.; Sharma, P.; Poddar, S.; Ducharme, S.; Gruverman, A.; Yang, Y.; Huang, J. Efficiency Enhancement in Organic Solar Cells with Ferroelectric Polymers. *Nat. Mater.* **2011**, *10*, 296–302.
15. Li, G.; Zhu, R.; Yang, Y. Polymer Solar Cells. *Nat. Photonics* **2012**, *6*, 153–161.
16. He, Z.; Zhong, C.; Su, S.; Xu, M.; Wu, H.; Cao, Y. Enhanced Power-Conversion Efficiency in Polymer Solar Cells Using an Inverted Device Structure. *Nat. Photonics* **2012**, *6*, 591–595.
17. Kaltenbrunner, M.; White, M. S.; Glowacki, E. D.; Sekitani, T.; Someya, T.; Sariciftci, N. S.; Bauer, S. Ultrathin and Lightweight Organic Solar Cells with High Flexibility. *Nat. Commun.* **2012**, *3*, 770.
18. Brown, T. M.; De Rossi, F.; Di Giacomo, F.; Mincuzzi, G.; Zardetto, V.; Realea, A.; Di Carlo, A. Progress in Flexible Dye Solar Cell Materials, Processes and Devices. *J. Mater. Chem. A* **2014**, *2*, 10788–10817.
19. Miyasaka, T. Toward Printable Sensitized Mesoscopic Solar Cells: Light-Harvesting Management with Thin TiO_2 Films. *J. Phys. Chem. Lett.* **2011**, *2*, 262–269.
20. Li, Y.; Lee, W.; Lee, D.-K.; Kim, K.; Park, N.-G.; Ko, M. J. Pure Anatase TiO_2 "Nanoglue": An Inorganic Binding Agent to Improve Nanoparticle Interconnections in the Low-Temperature Sintering of Dye-Sensitized Solar Cells. *Appl. Phys. Lett.* **2011**, *98*, 103301–103303.
21. Li, Y.; Lee, D.-K.; Kim, J. Y.; Kim, B.; Park, N.-G.; Kim, K.; Shin, J.-H.; Choi, I.-S.; Ko, M. J. PVDF-Nanofiber-Reinforced TiO_2 Photoelectrodes. *Energy Environ. Sci.* **2012**, *5*, 8950–8957.
22. Li, Y.; Yoo, K.; Lee, D. K.; Kim, J. Y.; Kim, H.; Kim, B.; Ko, M. J. Photovoltaic Properties of High Efficiency Plastic Dye-Sensitized Solar Cells Employing Interparticle Binding Agent "Nanoglue". *Nanoscale* **2013**, *5*, 4711–4719.
23. Yoon, J.; Li, L.; Semichaevsky, A. V.; Ryu, J. H.; Johnson, H. T.; Nuzzo, R. G.; Rogers, J. A. Flexible Concentrator Photovoltaics Based on Microscale Silicon Solar Cells Embedded in Luminescent Waveguides. *Nat. Commun.* **2011**, *2*, 1–8.
24. Fakharuddin, A.; Jose, R.; Brown, T. M.; Fabregat-Santiago, F.; Bisquert, J. A Perspective on the Production of Dye-Sensitized Solar Modules. *Energy Environ. Sci.*, in press.
25. Nakade, S.; Matsuda, M.; Kambe, S.; Saito, Y.; Kitamura, T.; Sakata, T.; Wada, Y.; Mori, H.; Yanagida, S. Dependence of TiO_2 Nanoparticle Preparation Methods and Annealing Temperature on the Efficiency of Dye-Sensitized Solar Cells. *J. Phys. Chem. B* **2002**, *106*, 10004–10010.
26. *Dye Sensitized Cell Markets 2012, Nano-531*; NanoMarkets, LC: Glen Allen, VA, USA, April 2012.
27. Fan, X.; Wang, F.; Chu, Z.; Chen, L.; Zhang, C.; Zou, D. Conductive Mesh Based Flexible Dye-Sensitized Solar Cells. *Appl. Phys. Lett.* **2007**, *90*, 073501.
28. Fu, Y.; Lv, Z.; Hou, S.; Wu, H.; Wang, D.; Zhang, C.; Zou, D. TCO-Free, Flexible, and Bifacial Dye-Sensitized Solar Cell Based on Low-Cost Metal. *Adv. Energy Mater.* **2012**, *2*, 37–41.
29. Cha, S. I.; Kim, Y.; Hwang, K. H.; Shin, Y.-J.; Seo, S. H.; Lee, D. Y. Dye-Sensitized Solar Cells on Glass Paper: TCO-Free Highly Bendable Dye-Sensitized Solar Cells Inspired by the Traditional Korean Door Structure. *Energy Environ. Sci.* **2012**, *5*, 6071–6075.
30. Yun, H. G.; Kim, M.; Kang, M. G.; Lee, I. H. Cost-Effective Dye-Sensitized Solar Cells Consisting of Two Metal Foils Instead of Transparent Conductive Oxide Glass. *Phys. Chem. Chem. Phys.* **2012**, *14*, 6448–6451.
31. Fu, D.; Lay, P.; Bach, U. E. TCO-Free Flexible Monolithic Back-Contact Dye-Sensitized Solar Cells. *Energy Environ. Sci.* **2013**, *6*, 824–829.
32. Cho, T.-Y.; Han, C.-W.; Yoon, S.-G. Transparent Conducting Oxide Free Dye Sensitized Solar Cell Using Flexible Stainless Steel Mesh. *J. Alloys Compd.* **2013**, *578*, 609–612.

33. Yoo, B.; Kim, K.-J.; Kim, Y. H.; Kim, K.; Ko, M. J.; Kim, W. M.; Park, N.-G. Titanium Nitride Thin Film As a Novel Charge Collector in TCO-Less Dye-Sensitized Solar Cell. *J. Mater. Chem.* **2011**, *21*, 3077–3084.
34. Kang, M. G.; Park, N.-G.; Ryu, K. S.; Chang, S. H.; Kim, K.-J. A 4.2% Efficient Flexible Dye-Sensitized TiO_2 Solar Cells Using Stainless Steel Substrate. *Sol. Energy Mater. Sol. Cells.* **2006**, *90*, 574–581.
35. Ito, S.; Ha, N.-L. C.; Rothenberger, G.; Liska, P.; Comte, P.; Zakeeruddin, S. M.; Péchy, P.; Nazeeruddin, M. K.; Gratzel, M. High-Efficiency (7.2%) Flexible Dye-Sensitized Solar Cells with Ti-Metal Substrate for Nanocrystalline-TiO_2 Photoanode. *Chem. Commun.* **2006**, 4004–4006.
36. Fabregat-Santiago, F.; Bisquert, J.; Palomares, E.; Otero, L.; Kuang, D.; Zakeeruddin, S. M.; Grätzel, M. Correlation between Photovoltaic Performance and Impedance Spectroscopy of Dye-Sensitized Solar Cells Based on Ionic Liquids. *J. Phys. Chem. C* **2007**, *111*, 6550–6560.
37. Adachi, M.; Sakamoto, M.; Jiu, J.; Ogata, Y.; Isoda, S. Determination of Parameters of Electron Transport in Dye-Sensitized Solar Cells Using Electrochemical Impedance Spectroscopy. *J. Phys. Chem. B* **2006**, *110*, 13872–13880.
38. Bisquert, J. Theory of the Impedance of Electron Diffusion and Recombination in a Thin Layer. *J. Phys. Chem. B* **2002**, *106*, 325–333.
39. Zhao, D.; Peng, T.; Lu, L.; Cai, P.; Jiang, P.; Bian, Z. Effect of Annealing Temperature on the Photoelectrochemical Properties of Dye-Sensitized Solar Cells Made with Mesoporous TiO_2 Nanoparticles. *J. Phys. Chem. C* **2008**, *112*, 8486–8494.
40. Koo, H.-J.; Park, J.; Yoo, B.; Yoo, K.; Kim, K.; Park, N.-G. Size-Dependent Scattering Efficiency in Dye-Sensitized Solar Cell. *Inorg. Chim. Acta* **2008**, *361*, 677–683.
41. Koo, H. J.; Kim, Y. J.; Lee, Y. H.; Lee, W. I.; Kim, K.; Park, N. G. Nano-Embossed Hollow Spherical TiO_2 As Bifunctional Material for High-Efficiency Dye-Sensitized Solar Cells. *Adv. Mater.* **2008**, *20*, 195–199.
42. Arakawa, H.; Yamaguchi, T.; Sutou, T.; Koishi, Y.; Tobe, N.; Matsumoto, D.; Nagai, T. Efficient Dye-Sensitized Solar Cell Sub-Modules. *Curr. Appl. Phys.* **2010**, *10*, S157–S160.
43. Roy-Mayhew, J. D.; Bozym, D. J.; Punckt, C.; Aksay, I. A. Functionalized Graphene as a Catalytic Counter Electrode in Dye-Sensitized Solar Cells. *ACS Nano* **2010**, *4*, 6203–6211.
44. Wu, M.; Lin, X.; Wang, Y.; Wang, L.; Guo, W.; Qi, D.; Peng, X.; Hagfeldt, A.; Gratzel, M.; Ma, T. Economical Pt-Free Catalysts for Counter Electrodes of Dye-Sensitized Solar Cells. *J. Am. Chem. Soc.* **2012**, *134*, 3419–3428.
45. Kavan, L.; Yum, J. H.; Grätzel, M. G.; Heyrovsky, J. Optically Transparent Cathode for Dye-Sensitized Solar Cells Based on Graphene Nanoplatelets. *ACS Nano* **2011**, *5*, 165–172.
46. Kim, J.-Y.; Kim, J. Y.; Lee, D.-K.; Kim, B.; Kim, H.; Ko, M. J. Importance of 4-tert-Butylpyridine in Electrolyte for Dye-Sensitized Solar Cells Employing SnO_2 Electrode. *J. Phys. Chem. C* **2012**, *116*, 22759–22766.
47. Hu, L.; Kim, H. S.; Lee, J.-Y.; Peumans, P.; Cui, Y. Scalable Coating and Properties of Transparent, Flexible, Silver Nanowire Electrodes. *ACS Nano* **2010**, *4*, 2955–2963.
48. Ran, Y.; He, W.; Wang, K.; Ji, S.; Ye, C. A One-Step Route to Ag Nanowires with a Diameter below 40 nm and an Aspect Ratio above 1000. *Chem. Commun.* **2014**, *50*, 14877–14880.
49. Lee, M. M.; Teuscher, J.; Miyasaka, T.; Murakami, T. N.; Snaith, H. J. Efficient Hybrid Solar Cells Based on Meso-Superstructured Organometal Halide Perovskites. *Science* **2012**, *338*, 643–647.
50. Kim, H.-S.; Lee, C.-R.; Im, J.-H.; Lee, K.-B.; Moehl, T.; Marchioro, A.; Moon, S.-J.; Humphry-Baker, R.; Yum, J.-H.; Moser, J. E.; *et al.* Lead Iodide Perovskite Sensitized All-Solid-State Submicron Thin Film Mesoscopic Solar Cell with Efficiency Exceeding 9%. *Sci. Rep.* **2012**, *2*, 591.
51. Ito, S.; Nazeeruddin, M. K.; Liska, P.; Comte, P.; Charvet, R.; Péchy, P.; Jirousek, M.; Kay, A.; Zakeeruddin, S. M.; Grätzel, M. Photovoltaic Characterization of Dye-Sensitized Solar Cells: Effect of Device Masking on Conversion Efficiency. *Prog. Photovoltaics* **2006**, *14*, 589–601.